ELSEVIER

Journal of Nuclear Materials 307–311 (2002) 60–68

journal of nuclear materials

www.elsevier.com/locate/jnucmat

Macroscopic erosion of divertor and first wall armour in future tokamaks

H. Würz [a,*], B. Bazylev [b], I. Landman [c], S. Pestchanyi [c], V. Safronov [c]

[a] *Forschungszentrum Karlsruhe, IHM, Postfach 3640, 76021 Karlsruhe, Germany*
[b] *Luikov Institute of Heat and Mass Transfer, 220072 Minsk, Belarus*
[c] *Troitsk Institute for Innovation and Fusion Research, 142190 Troitsk, Russia*

Abstract

Sputtering, evaporation and macroscopic erosion determine the lifetime of the 'in vessel' armour materials CFC, tungsten and beryllium presently under discussion for future tokamaks. For CFC armour macroscopic erosion means brittle destruction and dust formation whereas for metallic armour melt layer erosion by melt motion and droplet splashing. Available results on macroscopic erosion from hot plasma and e-beam simulation experiments and from tokamaks are critically evaluated and a comprehensive discussion of experimental and numerical macroscopic erosion and its extrapolation to future tokamaks is given. Shielding of divertor armour materials by their own vapor exists during plasma disruptions. The evolving plasma shield protects the armour from high heat loads, absorbs the incoming energy and reradiates it volumetrically thus reducing drastically the deposited energy. As a result, vertical target erosion by vaporization turns out to be of the order of a few microns per disruption event and macroscopic erosion becomes the dominant erosion source.

1. Introduction

This paper will give a comprehensive discussion on status and further activities on macroscopic erosion and erosion by evaporation of the high heat flux armour materials CFC, tungsten and beryllium. Presently CFC is considered as armour material for the vertical target in the divertor strike point region where high heat loads are expected during off-normal events [1]. Most part of the divertor including the upper parts of the vertical targets, the dome and the baffles are foreseen to be made from tungsten. The first wall (FW) armour choice presently is beryllium. Pulsed high heat load experiments with volumetric heating at e-beam facilities clearly show the existence of brittle destruction of graphite and CFCs and of dust production [2–4] and melt layer erosion of metals [4–6]. High heat load experiments with pulsed surface heat loads at plasma gun facilities and with quasi-stationary heating in tokamaks show the existence of melt layer erosion [7–9] and give some indications for brittle destruction of graphite [10–12]. A critical analysis of experimental results indicating brittle destruction was performed. Results of a 2-D numerical simulation of brittle destruction and of a simple estimation of macroscopic erosion based on a threshold value for the absorbed specific energy of 10 kJ/g for onset of this erosion [4] are presented. The absorbed energy is obtained from a solution of the 2-D heat conductivity equation with the three moving boundaries for evaporation, for melt front propagation and for brittle destruction. The velocity of the evaporation front is calculated using a non-steady state model of surface evaporation based on a kinetic model of the vapor expansion inside of the Knudsen layer as described in [13]. The energy deposition of electrons is calculated by 3-D Monte Carlo [14]. The 2-D numerical simulation of brittle destruction is based on modeling of the graphite lattice and calculation of cracking of intergranular bonds by thermal shocks [15]. Crack propagation into the depth of the sample

* Corresponding author. Tel.: +49-7247 82 3619; fax: +49-7247 82 4874.
E-mail address: hermann.wuerz@ihm.fzk.de (H. Würz).

0022-3115/02/$ - see front matter © 2002 Published by Elsevier Science B.V.
PII: S0022-3115(02)00938-8

produces individual open pits of large depth, when combining large macroscopic erosion occurs which determines the CFC armour lifetime. Metals show melt layer erosion by melt motion driven by external forces [16]. This results in an almost complete loss of the melt layer, formation of rather deep erosion craters mountains at the crater edge and considerable droplet splashing [17]. Boiling and bubble collapse and evolving surface waves due to a Kelvin Helmholtz instability might add to the surface roughness in metals and to droplet splashing [16]. The large surface roughness due to the shallow toroidal plasma impact act as hot spots receiving up to a factor of 30 higher heat loads than the plane surface. Enhanced impurity production at hot spots, at leading edges and at redeposited layers which consist of mixed materials with drastically reduced heat conductivity has the potential to limit the tolerable ELM energy to values considerably below what is specified for virgin armour materials [18].

The impact of runaway electrons is discussed in [16] and therefore is omitted here. The discussion on damage analysis focuses on surface and surface near effects. Arcing as an additional erosion source is not included [19]. Development of armour material and thermal analysis of the high heat flux components in which the armour material is brazed to a metallic heat sink are not discussed. Here reference is made to the literature, see for instance [20–22].

2. Brittle destruction and macroscopic erosion of graphite

2.1. Experimental evidence for brittle destruction

Results from erosion experiments with graphite targets performed at electron-beam facilities [2–4] demonstrate clearly that for pulsed volumetric heating brittle destruction occurs resulting in macroscopic erosion and emission of considerable amounts of dust [4,23]. In these experiments target screening by the evaporated material is of no concern, target screening by the dust particles exists but its influence because of rapidly decreasing density with ongoing time is not significant as discussed in [24]. Early erosion experiments were performed for samples from fine grain graphite IG-430U and from CFC CX-2002U at the JEBIS facility [2]. The energy of the electrons impacting perpendicular onto the target was 100 keV, the moderate peak target heat load was 0.41 GW/m^2 and the heat load duration was up to 60 ms. Fig. 1(a) shows a comparison of measured and calculated peak erosion by evaporation for the CFC sample. In the calculations evaporation of up to five atomic carbon clusters are taken into account [25]. According to the calculation the absorbed energy at 60 ms reaches 9.2 kJ/g remains all the time below the threshold for brittle destruction and thus brittle destruction is not occurring in agreement with the experimental results. For the calculation the realistic power density profile of the impacting electron beam was used. After exposure open pits were observed at the sample. However the pit density is not known. Fig. 1(b) shows a comparison of measured total erosion and calculated erosion by evaporation for the IG-430U sample with a smaller heat conductivity. The total erosion above 14 MJ/m^2 of absorbed energy due to onset of brittle destruction becomes larger than the calculated value for evaporation only. According to results from surface analysis the surface gets a rather large porosity indicating brittle destruction. The calculated temperature evolution in the bulk fine grain sample is shown in Fig. 2. Because of volumetric heating there is a temperature maximum inside of the sample where intense crack formation starts.

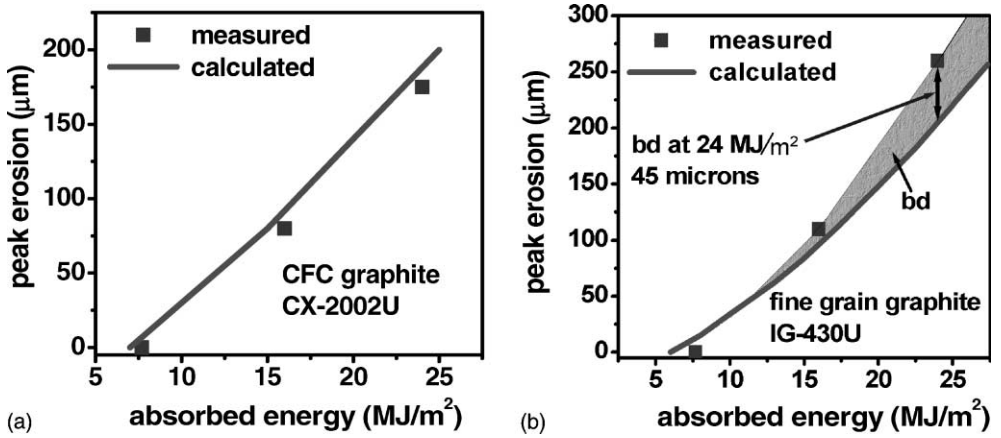

Fig. 1. (a) Comparison of measured total and calculated erosion by evaporation only for a CFC sample at the e-beam facility JEBIS. Sample heating was with 100 keV electrons of peak power density of 0.41 GW/m^2. (b) Comparison of measured total and calculated erosion by evaporation only for an IG-430U sample at JEBIS. The same heating conditions as for Fig. 1(a).

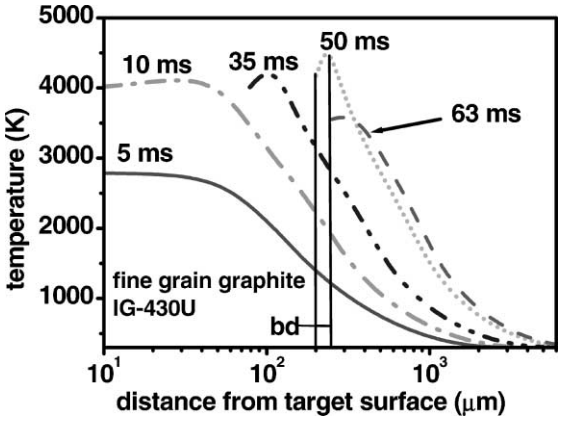

Fig. 2. Calculated evolution of temperature profiles for the sample IG-430U under the heat load conditions of Fig. 1(a). At 50 ms macroscopic erosion occurs.

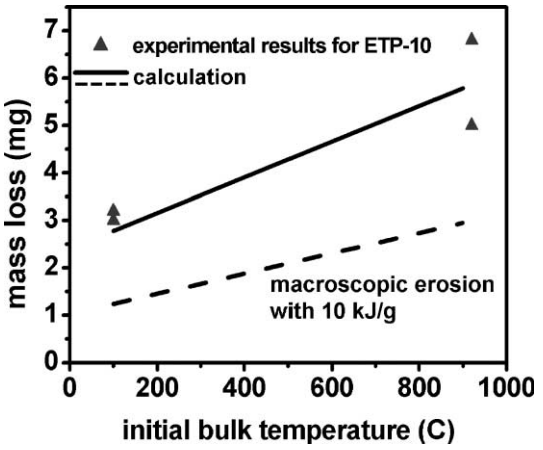

Fig. 3. Comparison of calculated and measured temperature dependence of total mass loss for an ETP-10 graphite sample for JEBIS conditions with 70 keV e-beam, the absorbed heat flux is 1.8 GW/m^2, the pulse duration is 2 ms.

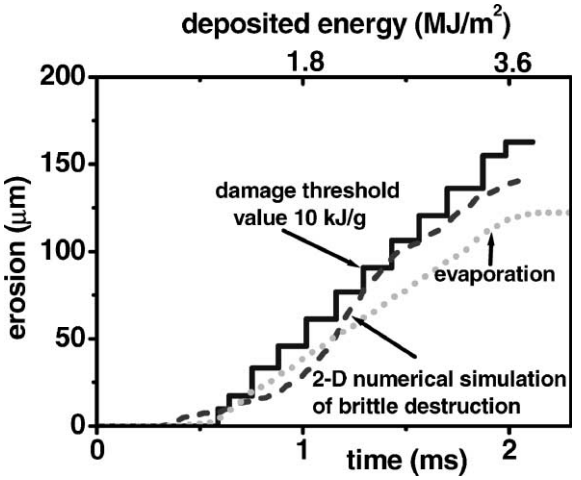

Fig. 4. Calculated erosion rates by evaporation and brittle destruction using a damage threshold value of 10 kJ/g for JEBIS conditions for an ETP-10 isotropic graphite sample and calculated erosion rates by brittle destruction. Initial sample temperature is 1000 °C.

The threshold value 10 kJ/g for onset of brittle destruction is reached after about 50 ms and due to crack propagation to the surface the overlaying layer is removed completely. According to the calculation macroscopic erosion contributes at 24 MJ/m^2 with 45 μm to the calculated total erosion of 260 μm which is in agreement with the measured value. The surface temperature as seen from Fig. 2 for 50 ms is above the sublimation temperature of 4000 K and even increases with time due to heat flowing from the temperature maximum to the surface. Due to the high surface temperature erosion is dominated by evaporation. With ongoing time the surface due to the moving evaporation front changes its position as can be seen from the temperature profiles.

Another situation occurs for pulsed high heat loads. A comparison of measured and calculated total mass loss values again for JEBIS now for 70 keV electrons is shown in Fig. 3 for an ETP-10 isotropic graphite sample for different sample temperatures. In this case the energy deposition of the electrons shows a maximum at a depth of 20 μm. Heating of the near surface layer was done with a heat flux of 1.8 GW/m^2 for 2 ms [26]. For the calculation a Gaussian power density profile with half-width of 5 mm was used. The heat conductivity of the sample is 100 W/mK at room temperature. The calculated mass loss due to brittle destruction is also shown in Fig. 3. For the 1000 °C sample macroscopic erosion accounts for about 50% of the mass loss and in terms of peak erosion for about 60% of total erosion as is seen from Fig. 4 showing the calculated erosion rates for evaporation and brittle destruction at the position of the peak target heat load. After 0.5 ms the surface temperature is above 4000 K. Brittle destruction occurs for the first time after 0.5 ms as is seen from Fig. 4. Due to the high heat load the threshold value for brittle destruction is permanently reached at later times and thus macroscopic erosion occurs during 1.5 ms. Total erosion in these experiments with volumetric heating mainly depends on the heat conductivity of the different samples. Therefore CFC and the other types of graphite show comparable total erosion and thus also comparable macroscopic erosion by brittle destruction for identical heat conductivities and heating conditions.

Volumetric heating in a tokamak only occurs during run away electron impact. If CFC armour is exposed quite large macroscopic erosion occurs [16]. Hot plasma heating of the armour is the dominating heating scenario

in a tokamak and this is surface heating. In this case macroscopic erosion can only develop if intense crack formation starts at temperatures considerably below the sublimation temperature of 4000 K, because when reaching this value intense evaporation starts and this would dominate the erosion. For pulsed high surface heat loads typical for the thermal quench phase of a disruption the total external pressure from the impacting hot plasma and from the vapor cloud gets at least 5 bar thus shifting the start of the sublimation to temperatures above 4500 K [27]. In this case macroscopic erosion might be able to compete with evaporation. Cracks as the starting mechanism for brittle destruction because of propagation into the depth of the sample might accumulate under the surface for quasi-stationary and cyclic heat loads. Such a pre-damaging when occurring in the course of repetitive heating might result in a considerable reduction of the brittle destruction threshold and then macroscopic erosion will dominate erosion also for surface heating. Such a mechanism presently is under investigation for pulsed and quasi-stationary surface heat loads. Fig. 5(a) shows SEM images of the CFC material SEP NB31, exposed to cyclic pulsed surface heat loads with hot plasma streams in the plasma gun facility MK-200 UG [12]. The target was perpendicular to the impacting hot plasma. The deposited energy is 15 MJ/m^2, however the duration of the heat load is only about 30 μs. After 40 shots large open pits with lengths up to 1 mm and at least 100 μm deep covering about 4% of the sample surface are to be seen. The size of the pits has to be compared with the typical erosion by evaporation which after 40 shots reaches about 15 μm. From dust particles collected outside of the impacting hot plasma the typical particle size was determined to be only of a few micron size [7,12]. This does not fit to the observed size of the pits. Therefore brittle destruction is a multicycle process initiated along the cracks which are propagating into the material. The Si doped CFC material SEP NS31 was also exposed to the same cyclic heat loads. In this material (1–1.5 at. wt% of Si) melting and evaporation of Si might produce local defects which might act as pit formation sites. However as seen from Fig. 5(b) the open pits produced during heat load exposure look rather similar. The only difference is the occurrence of bubbles during the first few exposures from boiling Si. Their disappearance after 10 exposures indicates that all Si was evaporated. Increasing the cyclic heating up to 80 exposures resulted in an increase of the

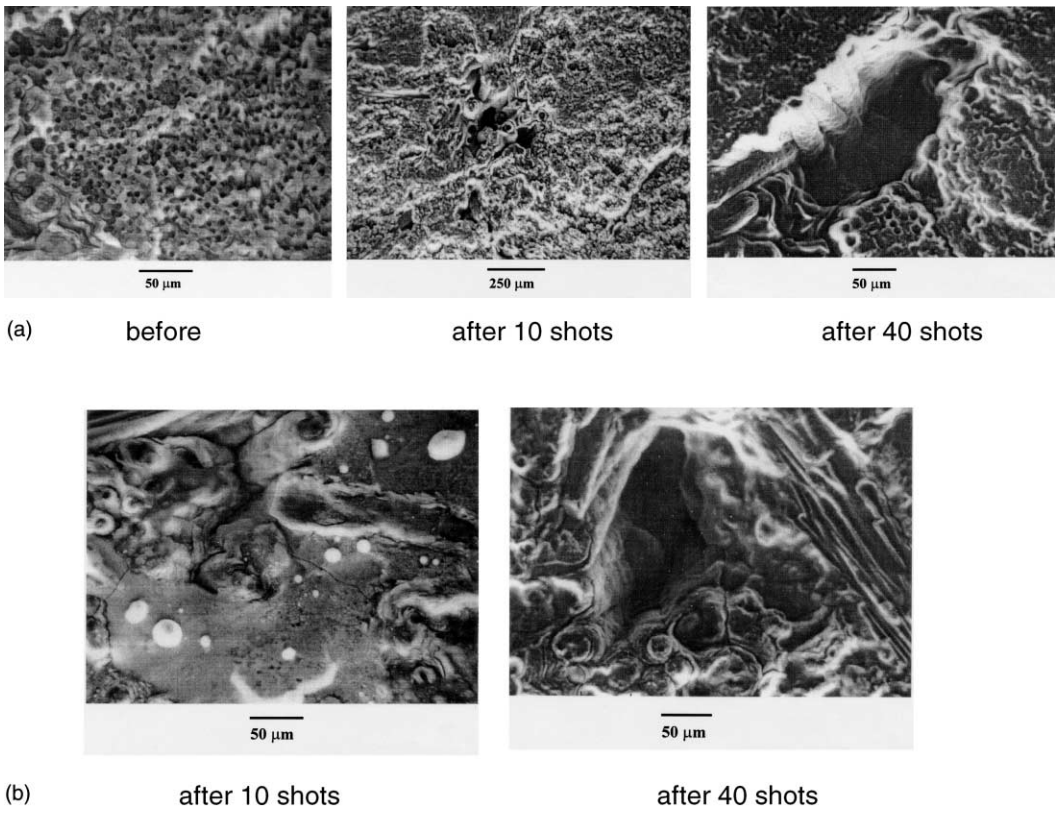

Fig. 5. SEM images of the (a) CFC sample SEP NB31 exposed to pulsed cyclic heat loads at the plasma gun facility MK-200 UG; (b) Si doped CFC sample SEP NS31.

particle size by a factor of 2 and in an increase of the density of the open pits. This might indicate an arising pre-damaging effect. However macroscopic erosion was not observed even after 80 shots. This indicates that for such pulsed surface heat loads of rather short duration the damage threshold for brittle destruction remains high and evaporation dominates as long as there is no degradation of material properties.

Very few experimental indications of brittle destruction of graphite armour in tokamaks are also available. In DIII-D a fine grain graphite sample was exposed to only one heat pulse with 50 MW/m^2 during 0.6 s simulating a leading edge [10] and in TEXTOR-94 a Si doped CFC limiter made from SEP NS31 was exposed to 26 shots with power loads of 12–14 MW/m^2 for 3 s [11]. In the DIII-D and the TEXTOR-94 samples rather large open pits with depth of up to 150 μm were observed. After 26 exposures, some of them ending in disruptions, the TEXTOR sample showed a factor of 3.5 larger density of pits compared with the initial density [28]. Using the given heat loads the evolution of the surface temperature and of the absorbed energy was calculated. For the TEXTOR sample with a quasi-stationary heat load the calculated surface temperature reaches about 2600 K corresponding to less than 6 kJ/g of absorbed energy. This rather low threshold value might indicate that single pits are formed at positions where defects are existing in the sample. The observed large depth of the pits clearly demonstrates crack propagation into the material what finally might result in rather large macroscopic erosion when single pits combine. Unfortunately erosion profiles were not measured and due to the rather moderate heat load and the limited number of exposures macroscopic erosion was not observed.

2.2. Numerical simulation of brittle destruction

For understanding of open pit formation with crack propagation, for estimating the potential of sample predamaging and for quantification of macroscopic erosion under surface heat loads a 2-D numerical simulation model was developed [15]. Thermal stress in a heated graphite sample due to the anisotropic properties of graphite might result in breaking of intergranular lattice bonds. As a consequence of intense cracking macroscopic layers are destroyed and graphite dust is produced. Important for brittle destruction to occur are the anisotropy of the graphite grains, the failure stress distribution of the bonds connecting adjacent grains and the temperature and its gradient in the bulk material. Cracks preferentially are propagating into the depth of the sample rendering brittle destruction the potential for large macroscopic erosion. Therefore the analysis of brittle destruction is mandatory for a damage evaluation of CFC armour. Pores in the bulk are not considered presently. Annealing effects are modeled in such a way that the heat conductivity gets its original value when grains with broken bonds by thermal expansion are coming in contact again. The failure stress distribution was determined from compression tests which simulate volumetric heating. The 2-D numerical simulation model was tested for volumetric heating under JEBIS conditions. A comparison of calculated erosion rates by brittle destruction using the numerical simulation and the damage threshold value of 10 kJ/g is shown in Fig. 4 for an ETP-10 sample of initial temperature of 1000 °C.

Hot plasma heating of the divertor armour during the thermal quench phase of a disruption causes erosion by evaporation. During the time duration of the pulsed heat load of typically 10 ms with heat loads up to a few GW/m^2 the vapor shield which is formed drastically reduces the effective target heat load and reduces erosion by evaporation to a few microns [27]. The effective heat load as calculated with FOREV-2 was used for a first numerical simulation of pit formation and crack propagation for surface heating. Because of lack of data the same failure stress values as for volumetric heating were used. To get a handable simulation problem the sample size used in the calculations was limited to a surface length of 2 mm and a thickness of 0.7 mm thus allowing to simulate a single pit. Fig. 6 shows the calculated evolution of such a pit for an initial peak target heat load of 3 GW/m^2. Between the pulses cooling down of the sample to its initial temperature was assumed. Brittle destruction forms an open pit and the sample shows crack propagation into the bulk as indicated by the thin black lines at the bottom of the pit. Due to this predamaging the depth of the open pit increases during the next pulses as is seen from Fig. 6. Increasing the time duration of the heat pulse would increase the number of the pits and their depth. Another very first and preliminary numerical simulation was performed for a quasi-stationary heat load of 50 MW/m^2 with a time duration of up to 10 s in which surface temperatures of 3600 K are reached. Fig. 7 shows the pattern of broken bonds

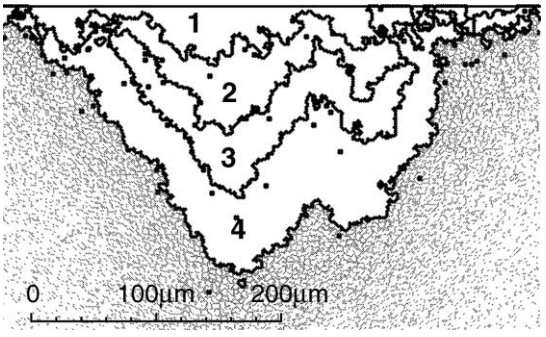

Fig. 6. Results from numerical simulation of evolution of size and depth of a single pit under pulsed cyclic surface heat loads simulating disruptions with 30 MJ/m^2 and duration of 10 ms.

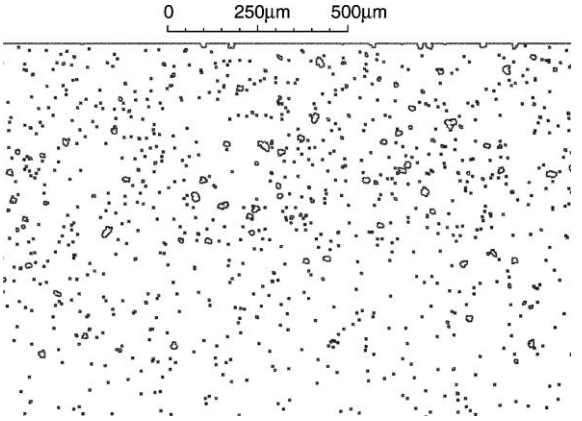

Fig. 7. Numerical simulation of formation of broken bonds in a CFC sample for a quasi-stationary heat load of 50 MW/m^2 corresponding to a surface temperature of 3600 K.

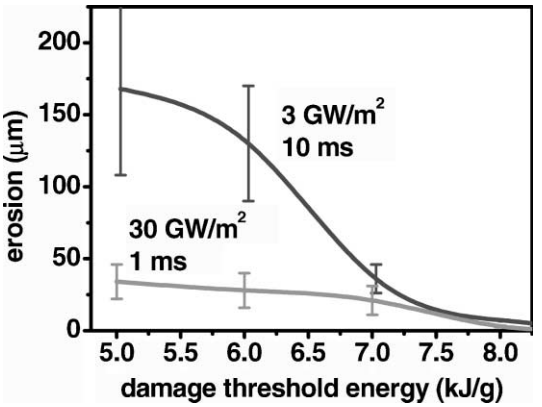

Fig. 8. Macroscopic erosion of vertical graphite armour for a pulsed heat load as function of the damage threshold energy.

after 10 s. Macroscopic cracks have not been developed but some damage exists inside of the sample up to a depth of about 1 mm. Assuming that the evaporated material does not form a vapor shield then the erosion by surface evaporation might get values of up to several mm and thus dominates total erosion. However with a vapor shield which only stops the impacting hot ions the erosion by evaporation drops down to a few microns. In this case macroscopic erosion if pre-damaging under cyclic heat loads continues might get the dominating erosion mechanism.

The 2-D simulation describes the formation and growth of single pits under surface heating. Actually pits may arise everywhere at the heated surface provided that the heating is intense enough for intense crack formation. If the overall pit density increases with ongoing heating a macroscopic erosion crater of considerable depth finally might arise. To describe this a 3-D simulation model which is presently under testing has to be applied. Moreover validated failure stress values have to be used for estimating macroscopic erosion for surface heat loads. Target shielding by the dust particles from brittle destruction is of no concern for the magnitude of the macroscopic erosion. The target shielding by dust particles only delays the formation process of the open pits and thus some more heat pulses with surface heating are necessary until the pits combine into macroscopic erosion.

2.3. Macroscopic erosion scenario under tokamak conditions

For pulsed and quasi-stationary surface heating it is presently not clear which damage threshold energy value has to be used for onset of macroscopic erosion. To demonstrate its importance macroscopic erosion was calculated for different damage threshold energy values simulating crack accumulation and pre-damaging. Assuming that open pit formation requires surface temperatures above 2500 K then brittle destruction is of no concern for normal (quasi-stationary) operation at well aligned armour tiles where heat loads typically are below 5 MW/m^2. Brittle destruction might occur during disruptions and as erosion at leading edges of gaps between armour tiles (gap width typically 5 mm) and of open pits with typical pit size of around 1 mm formed during disruptions. Calculated results on macroscopic erosion are shown in Fig. 8 for a vertical graphite target under hot plasma impact for the two different surface heat loads 3 and 30 GW/m^2 as typically occurring during disruptions corresponding to an energy density of 30 MJ/m^2. Macroscopic erosion occurs for damage threshold values below 8.5 kJ/g. This means only when a degradation of the mechanical and thermal properties of the armour material has occurred during preceding discharges then intense brittle destruction finally might develop in the predamaged sample. In this case macroscopic erosion will become quite large and will limit the armour lifetime. The error bars shown in Fig. 8 indicate the influence of the radiative energy transfer through the dust cloud region with two different absorption coefficients for radiation calculated from the estimated particle density and the cloud size.

3. Melt layer erosion of metals

Experimental results from e-beam and plasma gun facilities and from tokamaks demonstrate the existence of a rather pronounced radial motion in the melt layer from the center of the melted pool to the periphery [4–6,8,9]. As a result a considerable part of the melt layer is swept away, mountains of ejected melted material are formed at the crater edge and droplet splashing occurs.

During such off-normal events as disruptions and vertical displacement events (VDEs) the energy flux at the armour material might reach values sufficient for melting of metals and a thin melt layer might appear at the target surface. Melt motion driven by external forces also produces a considerable surface roughness and destroys any castellation thus increases the fatigue stress of the metallic armour. The numerical simulation of melt motion is based on a 1-D fluid dynamics model being described together with model validation against results from e-beam experiments in an accompanying paper to this conference [17].

3.1. Tokamak disruptions

A first application of numerical simulation of melt motion was done for hot plasma impact onto a vertical tungsten target. A typical disruption condition with a peak power density of 3 GW/m^2 and a time duration of 10 ms and with the separatrix strike point (SSP) downstream was used. Time dependent tungsten armour heat loads and plasma shield pressure profiles were calculated with FOREV-2. The pressure profiles of the plasma shield confined in the external magnetic field for more than 4 ms is between 4 and 7 bar and the pressure profiles show a half-width of only 4 cm as is shown in Fig. 9. The upstream shift of the pressure profiles follows the upstream movement of the heat load which is due to reradiation from the expanding plasma shield [27]. For the given target heat load the maximum static melt layer thickness is about 470 μm as shown in Fig. 10 with the upstream direction as positive and the downstream direction as negative direction. The melt profile because of the upstream shift of the heat load shows a rather constant depth over a length of 15 cm. The external pressure gradient from the plasma shield causes a

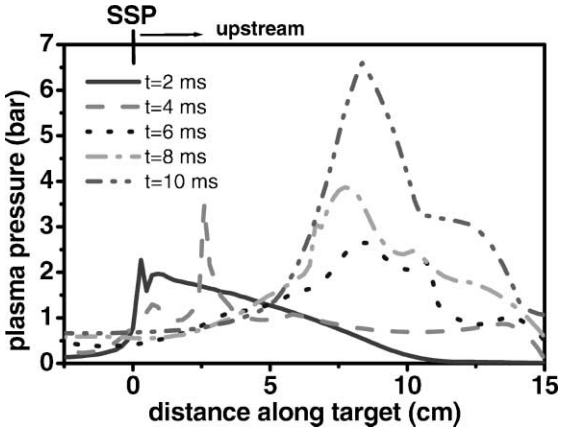

Fig. 9. Time dependent profiles of the external pressure from the plasma shield as calculated with FOREV-2 for a disruption case with 30 MJ/cm^2 and a time duration of 10 ms.

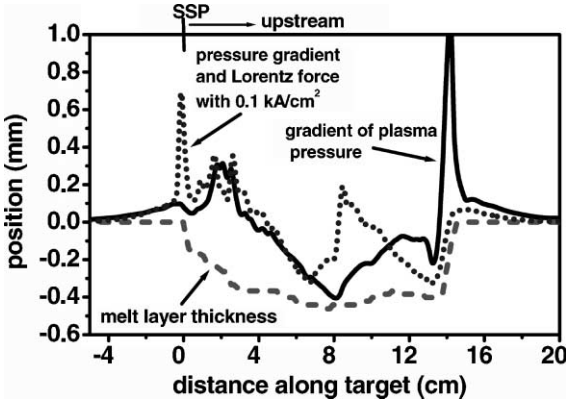

Fig. 10. Numerical results on crater depth for tungsten armour during a disruption with peak heat load of 3 GW/m^2 and time duration of 10 ms for the two different forces gradient of plasma pressure only and sum of plasma pressure and Lorentz force due to a current density of 0.1 kA/cm^2. For comparison the melt layer thickness without melt motion is also shown.

drastic melt layer erosion as shown in Fig. 10 with a rather symmetrical profile. The crater depth after resolidification is up to 410 μm and thus comparable to the melt layer thickness. In tokamaks during disruptions electric currents are flowing from the plasma into the structure [29]. The current density of that component crossing the melt layer perpendicularly to the target surface is typically 0.1–1 kA/cm^2. The resulting volumetric Lorentz force being parallel to the armour surface causes melt motion in either downstream or upstream direction depending on the direction of the toroidal magnetic field. Taking pressure gradient and Lorentz force due to a current of 0.1 kA/cm^2 into account results in a maximum crater depth of about 350 μm. For a current of 1 kA/cm^2 the maximum crater depth is 700 μm thus being up to a factor of 1.4 larger than the thickness of the melt layer. Calculated average melt velocities in the tungsten melt layer for the two forces pressure gradient and Lorentz force for a current of 0.1 kA/cm^2 are shown in Fig. 11. The Lorentz force results in larger melt velocities than the pressure gradient of the external plasma shield. For the direction of the toroidal magnetic field as chosen here both velocities close to the SSP are directed downstream and add together to values of up to 800 cm/s. As a consequence the crater profile becomes asymmetrical and the mountains depending on the direction of the toroidal magnetic field appear either at the down or upstream crater edge. Moreover due to the rather large melt velocity considerable droplet splashing will occur in the tungsten divertor armour (the Reynolds number becomes rather large and a turbulent flow can arise).

There might also exist a current flowing parallel to the armour surface. The resulting body force which is

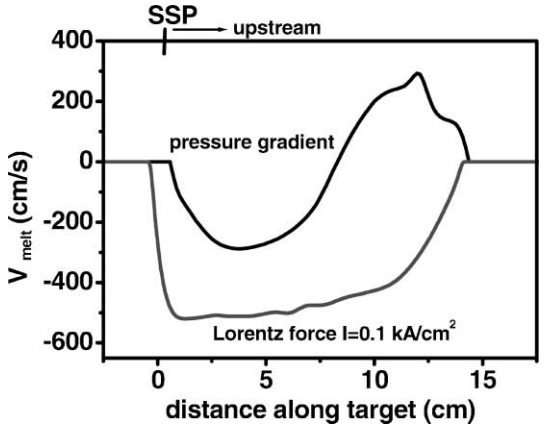

Fig. 11. Comparison of calculated average melt velocities in the tungsten melt layer for the two different forces Lorentz force with current density of 0.1 kA/cm^2 and gradient of plasma pressure. Close to the SSP both velocities are directed downstream.

perpendicular to the armour surface further amplifies the melt motion and contributes to droplet splashing.

3.2. Vertical displacement events

VDEs are heating the FW, the baffle and the dome armour via surface heat loads. For VDEs it is assumed that the energy density deposited to the structure is up to 30 MJ/m^2 per event. The maximum impact energy of the hot plasma is assumed to be 1 keV. The duration of the heat load is assumed to be 0.1 s. The heated area has a width of 30 cm with a constant power density. It is assumed further that the Halo current is up to 1 kA/cm^2 flowing into the structure during the event. Calculated crater profiles are shown in Fig. 12(a) and (b) for Beryllium. In Fig. 12(a) results are shown for two cases of the Halo current density with 0.1 and 1 kA/cm^2. Fig. 12(a) is valid for no armour shielding and for Fig. 12(b) it was assumed that the impacting plasma ions are stopped in an evolving plasma shield. The crater depth for both cases are rather comparable despite the fact that the static melt layer thickness in the case with ion shielding becomes only 250 μm. The positive velocity of the melt motion shifts the melt to the right. The maximum crater depth is 2.8 mm for a current density of 1 kA/cm^2 and 2 mm for 0.1 kA/cm^2 and thus drastically exceeds the static melt layer thickness which is 1 mm without shielding. Fig. 13 shows the calculated crater profiles for tungsten armour again without shielding for the same heating conditions. The maximum crater depth is up to 2 mm. Fig. 14 shows calculated melt velocities for Be and W armour. The high velocity causes considerable droplet splashing [30] by the evolving interfacial instability [31] of the film flow. Because of the higher

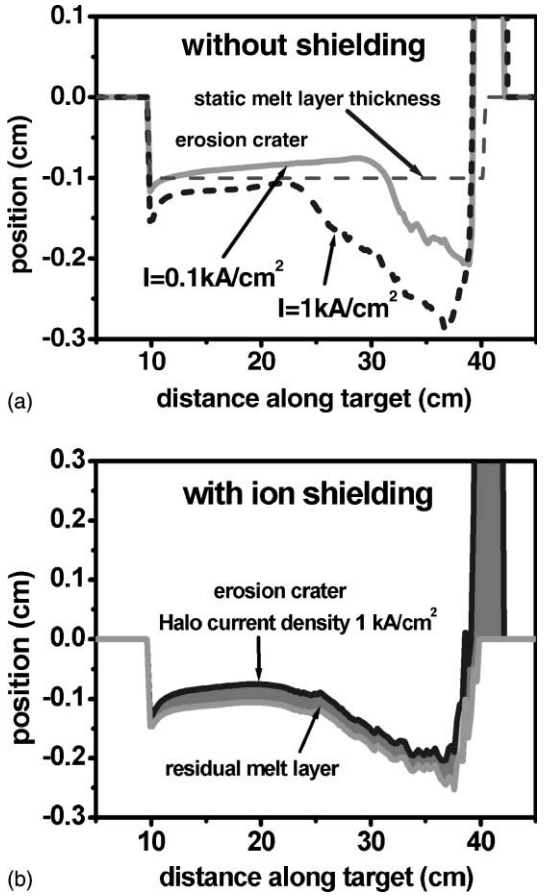

Fig. 12. (a) Calculated crater profiles in a Be FW armour for a VDE with 30 MJ/cm^2 and 0.1 s for the two values of the Halo current of 0.1 and 1 kA/cm^2 without shielding. (b) Calculated crater profiles for the same conditions as under (a) but with ion shielding.

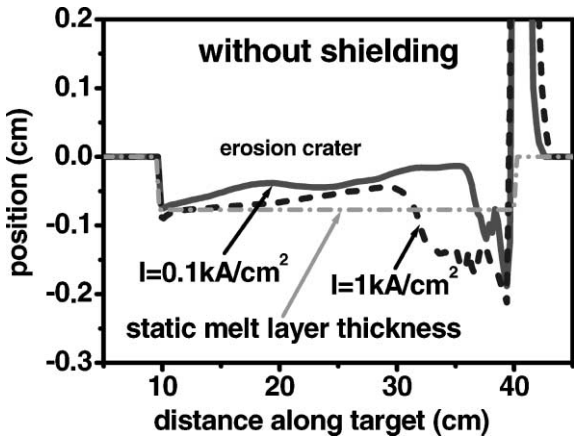

Fig. 13. Calculated crater profiles for a W FW armour for a VDE with 30 MJ/m^2 and 0.1 s without shielding.

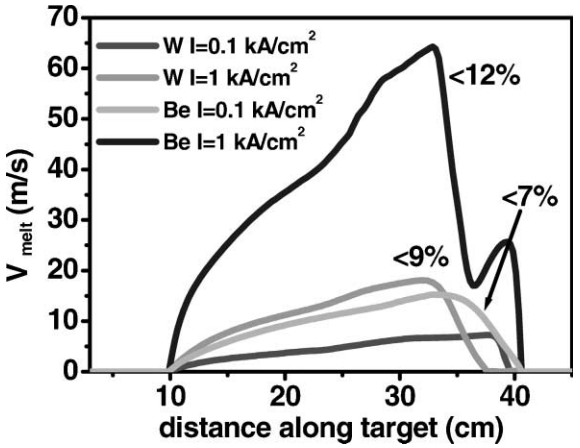

Fig. 14. Typical melt velocities for Be and W for a VDE with 30 MJ/m^2 and 0.1 s. The indicated numbers describe the fraction of the melted mass which is splashed by droplets.

velocity of the Be melt the droplet splashing there is larger. The given numbers at the curves describe the fraction of melted mass splashed away by droplets.

4. Conclusions

Melt layer erosion of metals is dominated by melt flow. Pressure gradients and Lorentz forces in the case of disruptions and only Lorentz forces in the case of VDEs trigger a pronounced melt motion which sweeps away a considerable part of the melt layer. For disruptions of 10 ms time duration the crater depth in the tungsten armour of a vertical target reaches 700 μm and the melt motion towards the crater edge is so violent that considerable droplet splashing occurs and any castellation will be destroyed by filling of the gaps with melted material. A moderate VDE on a Be FW armour results in crater depths of up to 2.8 mm and on a tungsten armour a depth of up to 2 mm. The high melt velocity results in considerable droplet splashing. Melt layer erosion at leading edges of metallic armour material and droplet splashing during normal operation produce hot spots. Enhanced impurity production at these hot spots limits the tolerable ELM energy to a level which is below what is tolerable for a virgin plane metallic armour target [32]. Therefore the use of any metallic armour in the divertor requires mitigation of disruptions and a tile arrangement which excludes leading edges. The use of Be as FW armour because of its large damage during VDEs becomes problematic.

Brittle destruction of CFC occurs for volumetric heating and its quantification by numerical modeling is possible. The potential of brittle destruction under pulsed and quasi-stationary cyclic surface heat loads presently is not clear. Available experimental results and results from numerical modeling indicate formation of open pits of rather large depth due to preferential crack propagation into the depth of the sample. However the minimum surface temperature required for intense pit formation and onset of macroscopic erosion under cyclic surface heat loads is not known. The large erosion potential of macroscopic erosion makes investigations on brittle destruction mandatory.

References

[1] G. Janeschitz, Fus. Eng. Des. 49&50 (2000) 107.
[2] M. Araki et al., Fus. Eng. Des. 19 (1992) 101.
[3] J. Linke et al., Fus. Eng. Des. 49&50 (2001) 235.
[4] V.T. Astrelin et al., Nucl. Fusion 37 (1997) 1541.
[5] K. Nakamura et al., Fus. Eng. Des. 39&40 (1998) 285.
[6] A. Lodato et al., Fus. Eng. Des. 49&50 (2000) 255.
[7] V. Safronov et al., J. Nucl. Mater. 290–293 (2001) 1052.
[8] B.J.D. Tubbing et al., 22nd EPs Bournemouth, 3–7 July 1994, vol. 19C, Part III 453.
[9] T. Tanabe et al., J. Nucl. Mater. 241–243 (1997) 116.
[10] O.I. Buzhinsky et al., J. Nucl. Mater. 266–269 (1999) 793.
[11] A. Huber et al., Phys. Scr. T 91 (2001) 61.
[12] N. Arkhipov et al., these Proceedings.
[13] H. Wuerz et al., Fus. Sci. Technol. 40 (2001) 191.
[14] G. Miloshevsky, H.Wuerz, 3-D Monte Carlo calculations of energy deposition into bulk graphite and into an inhomogeneous carbon plasma shield, Forschungszentrum Karlsruhe Report FZKA 6482, 2000.
[15] S. Pestchany, H. Wuerz, Phys. Scr. T 91 (2001) 84.
[16] H. Wuerz et al., J. Nucl. Mater. 290–293 (2001) 1138.
[17] B. Bazylev et al., these Proceedings.
[18] G. Janeschitz et al., J. Nucl. Mater. 290–293 (2001) 1.
[19] C. Garcia Rosales et al., 21 EPS Montpellier June 27–July 1, 1994, vol. 18B, part II 718.
[20] G. Vieider et al., Fus. Eng. Des. 49&50 (2000) 135.
[21] I. Smid et al., J. Nucl. Mater. 258–263 (1998) 160.
[22] V. Barabash et al., J. Nucl. Mater. 258–263 (1998) 149.
[23] H. Wuerz et al., 27th EPS Budapest, 12–16 June 2000.
[24] H. Wuerz et al., Fus. Eng. Des. 56&57 (2001) 349.
[25] C.H. Wu et al., J. Nucl. Mater. 258–263 (1998) 782.
[26] K. Nakamura et al., J. Nucl. Mater. 212–215 (1994) 1201.
[27] H. Wuerz et al., Damage evaluation of vertical targets and first walls during ITER-FEAT off-normal Events, Forschungszentrum Karlsruhe Report FZKA 658, 2001.
[28] A. Huber, IPP Juelich, private communication.
[29] J. Lingertat et al., J. Nucl. Mater. 214–243 (1997) 402.
[30] B.J. Azzopardi, Int. J. Multiphase Flow 23 (1997) 1.
[31] W. Shyy, R. Narayanan (Eds.), Fluid Dynamics at Interfaces, Cambridge University, Cambridge, 1999.
[32] S. Pestchanyi, H. Wuerz, I. Landman, Impurity production and edge plasma pollution during ITER-FEAT ELMs, Plasma Phys. Contr. Fus., accepted for publication.